2017

Microglial complement receptor 3 regulates brain Aβ levels through secreted proteolytic activity

Eva Czirr

John R. Cirrito

et al

Microglial complement receptor 3 regulates brain Aβ levels through secreted proteolytic activity

Eva Czirr,[1] Nicholas A. Castello,[4] Kira I. Mosher,[1] Joseph M. Castellano,[1,2] Izumi V. Hinkson,[1,2,3] Kurt M. Lucin,[1] Bernat Baeza-Raja,[4] Jae Kyu Ryu,[4] Lulin Li,[1,2,3] Sasha N. Farina,[1,3] Nadia P. Belichenko,[1] Frank M. Longo,[1] Katerina Akassoglou,[4,5] Markus Britschgi,[1] John R. Cirrito,[6,7,8] and Tony Wyss-Coray[1,2,3]

[1]Department of Neurology and Neurological Sciences and [2]Paul F. Glenn Center for the Biology of Aging, Stanford University School of Medicine, Stanford, CA 94305
[3]Center for Tissue Regeneration, Repair, and Restoration, Veterans Affairs Palo Alto Health Care System, Palo Alto, CA 94304
[4]Gladstone Institute of Neurological Disease and [5]Department of Neurology, University of California, San Francisco, San Francisco, CA 94158
[6]Department of Neurology, Washington University, St. Louis, MO 63110
[7]Knight Alzheimer's Disease Research Center, Washington University Medical Center, St. Louis, MO 63110
[8]Hope Center for Neurological Disorders, Washington University, St. Louis, MO 63110

Recent genetic evidence supports a link between microglia and the complement system in Alzheimer's disease (AD). In this study, we uncovered a novel role for the microglial complement receptor 3 (CR3) in the regulation of soluble β-amyloid (Aβ) clearance independent of phagocytosis. Unexpectedly, ablation of CR3 in human amyloid precursor protein–transgenic mice results in decreased, rather than increased, Aβ accumulation. In line with these findings, cultured microglia lacking CR3 are more efficient than wild-type cells at degrading extracellular Aβ by secreting enzymatic factors, including tissue plasminogen activator. Furthermore, a small molecule modulator of CR3 reduces soluble Aβ levels and Aβ half-life in brain interstitial fluid (ISF), as measured by in vivo microdialysis. These results suggest that CR3 limits Aβ clearance from the ISF, illustrating a novel role for CR3 and microglia in brain Aβ metabolism and defining a potential new therapeutic target in AD.

The Journal of Experimental Medicine

INTRODUCTION

Aberrant accumulation of the β-amyloid (Aβ) peptide in the brain parenchyma is widely hypothesized to initiate a pathogenic cascade leading to neuronal dysfunction and subsequent cognitive decline in Alzheimer's disease (AD; Hardy and Selkoe, 2002). The factors that underlie Aβ accumulation in sporadic AD are poorly understood. However, evidence indicates that impaired clearance is mainly responsible (Bateman et al., 2006; Roberts et al., 2014). Clearance of soluble Aβ is achieved by several mechanisms, including blood–brain barrier (BBB)–mediated transport, interstitial fluid (ISF) bulk flow, and cellular uptake and degradation. Disturbances in any of these pathways are likely to contribute to the development of Aβ accumulation. Removal of Aβ deposits is, in part, mediated through phagocytic cells in concert with immune recognition molecules (Lucin and Wyss-Coray, 2009; Czirr and Wyss-Coray, 2012). Indeed, microglia are now widely recognized to have important roles in neurodegeneration and in AD (Saijo and Glass, 2011). This notion has received genetic support from genome-wide association studies that have identified several single nucleotide polymorphisms in immune-related genes that increase the risk of developing late onset AD (Lambert et al., 2009; Jun et al., 2010; Naj et al., 2011; Guerreiro et al., 2013; Jonsson et al., 2013). In the brain, most of these genes are exclusively expressed in microglia, highlighting their importance in AD. Complement receptor 3 (CR3; CR3, CD11b/CD18, and Mac-1) is one of the major phagocytic receptors expressed on microglia (Ehlers, 2000) and is a dimeric receptor comprised of CD18 and its unique subunit CD11b (Ivashkiv, 2009; Linnartz and Neumann, 2013). The receptor is able to mediate Aβ phagocytosis (Fu et al., 2012), as well as the removal of synapses during development (Stevens et al., 2007; Schafer et al., 2012), in a model of neurodegeneration (Stevens et al., 2007) and in amyloid precursor protein (APP)–transgenic mice (Hong et al., 2016). Interestingly, levels of natural CR3 ligands, such as complement fragments, ICAM-1, and fibrin, are increased in AD patients (Shen et al., 2001; van Oijen et al., 2005; Ray et

Correspondence to Tony Wyss-Coray: twc@Stanford.edu

E. Czirr's present address is Alkahest Inc., San Carlos, CA 94070.

K.M. Lucin's present address is Eastern Connecticut State University, Willimantic, CT 06226.

M. Britschgi's present address is Roche Pharmaceutical Research and Early Development, Neuroscience Discovery, Roche Innovation Center Basel, 4070 Basel, Switzerland.

Abbreviations used: AD, Alzheimer's disease; APP, amyloid precursor protein; BBB, blood–brain barrier; CR3, complement receptor 3; ISF, interstitial fluid; LA-1, Leukadherin 1; MMP, matrix metalloproteinase; qPCR, quantitative PCR; tPA, tissue plasminogen activator.

The Rockefeller University Press $30.00
J. Exp. Med. 2017 Vol. 214 No. 4 1081–1092
https://doi.org/10.1084/jem.20162011

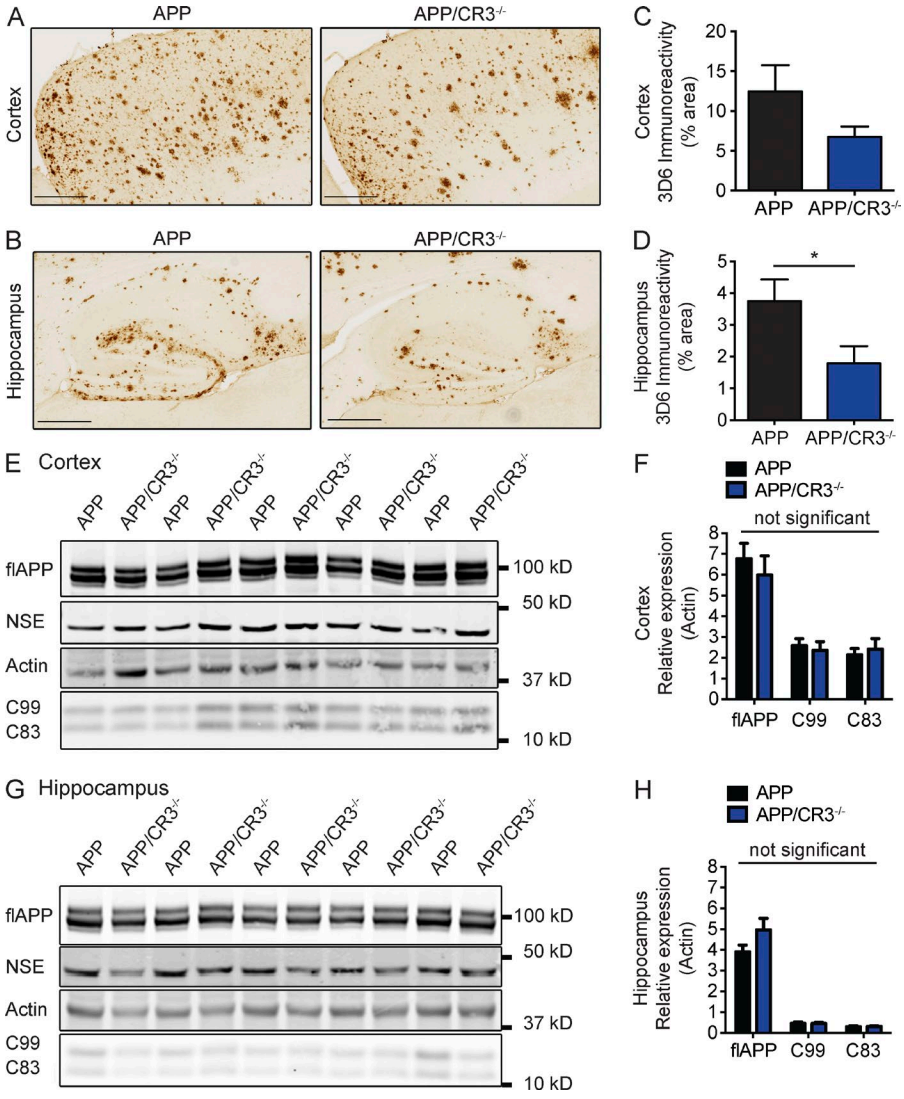

Figure 1. **Lack of CR3 results in reduced plaque deposition in APP transgenic mice while leaving APP expression and processing unaffected.** (A–D) Aβ staining in cortex (A) and hippocampus (B) of APP and APP/CR3$^{-/-}$ mice and quantification of Aβ immunoreactivity in cortex (C) and hippocampus (D). 12-mo-old mice were used. n = 8–9 mice per group and 6 sections per mouse. *, $P < 0.05$. Bars, 200 µm. (E and G) Western blots of cortical (E) and hippocampal (G) lysates showing full-length APP (flAPP) and C99 and C83 cleavage products, as well as β-actin and neuron-specific enolase (NSE) loading controls. (F and H) Quantification of Western blots in cortex (F) and hippocampus (H). (E–H) 3-mo-old male and female mice were used. n = 5 mice per group. Unpaired Student's t test was used. All values are mean ± SEM.

al., 2007; Xu et al., 2008; Ryu and McLarnon, 2009; Daborg et al., 2012; Bardehle et al., 2015).

Here, we identify a novel role for microglia and CR3 in the maintenance of Aβ homeostasis independent of phagocytosis. In the absence of CR3, Aβ deposition is reduced, and extracellular Aβ degradation is increased. Furthermore, modulating CR3 with the small molecule Leukadherin 1 (LA-1) increases Aβ degradation in vitro while reducing ISF Aβ levels and half-life in vivo. Together, these findings suggest that CR3 and microglia play an important role in Aβ homeostasis and identify a potential new therapeutic target in AD.

RESULTS

Genetic ablation of CR3 in APP-transgenic mice leads to reduced Aβ deposition

Human AD brains show an increase in complement proteins associated with plaques (Afagh et al., 1996; Yasojima et al., 1999). Complement proteins are important for removal of Aβ deposits, and interference with the central component C3 results in increased plaque deposition (Wyss-Coray et al., 2002; Maier et al., 2008). Microglial CR3 can target these deposits, and we initially hypothesized that lack of CR3 would result in higher Aβ plaque load because of reduced phagocytic activity. To test this hypothesis, we crossed mice deficient in its unique component CD11b (CR3$^{-/-}$; Soriano et al., 1999) with APP transgenic mice harboring two familial AD-associated APP mutations (Rockenstein et al., 2001). Surprisingly, the amount of Aβ deposition was decreased in 12-mo-old APP mice lacking CR3 (Fig. 1, A and B). Quantification of the percent Aβ-positive area showed a statistically significant decrease in plaque deposition in the hippocampus (Fig. 1 D) and a trend in the same direction in the cortex (Fig. 1 C), whereas expression of APP and its processing were unaffected (Fig. 1, E–H).

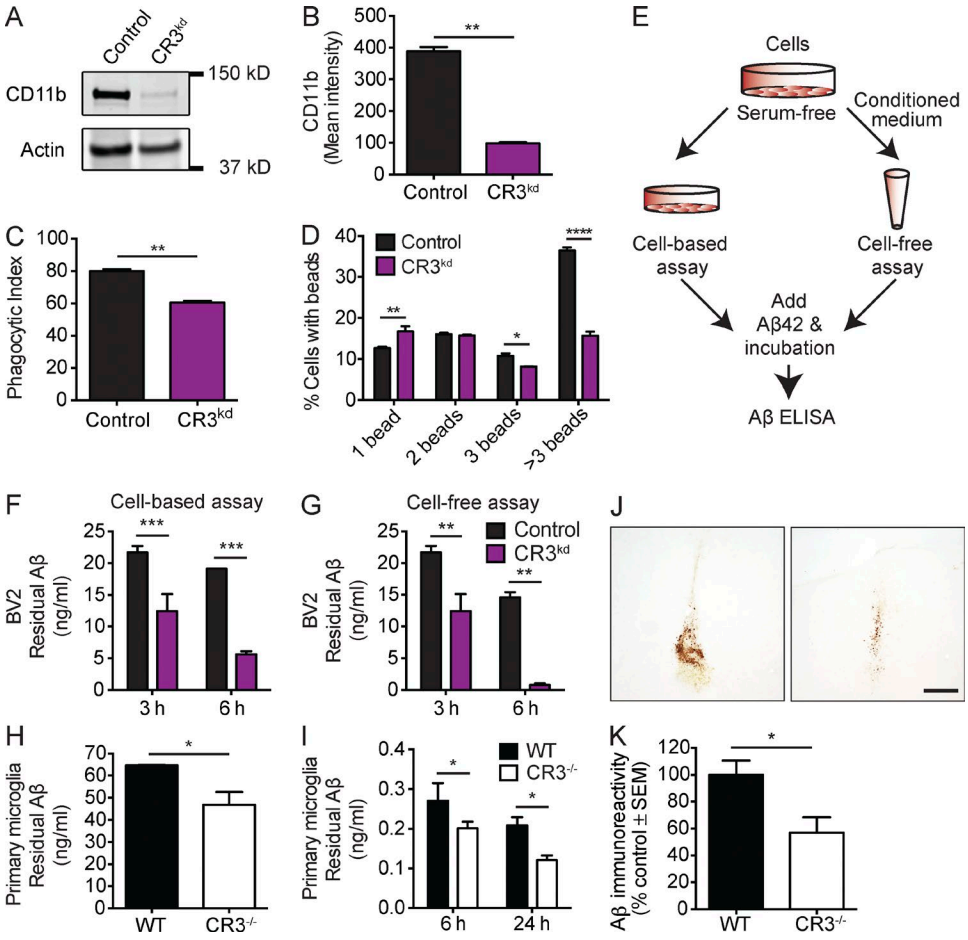

Figure 2. **CR3 deficiency leads to reduced phagocytic activity and increased Aβ degradation in vitro.** (A and B) Western blot (A) and flow cytometric quantification (B) of CD11b expression in CR3^{kd} and control BV2 cell lines. (B) $n = 2$ replicates. (C and D) Quantification of baseline phagocytosis activity (C) and phagocytosis efficiency (D) in control and CR3^{kd} BV2 cells. (E) Schematic of Aβ degradation assay. (F and G) Cell-based (F) and cell-free (G) Aβ degradation assays of control and CR3^{kd} cells were quantified. (H and I) Aβ degradation using primary adult microglia. (J and K) Aβ staining in hippocampus of mice stereotactically injected with Aβ42 (J) and quantification of residual immunoreactivity (K). 3–4-mo-old male and female mice were used. $n = 9$ per group. Bar, 200 µm. (C, D, and F–I) Representative graphs of three to five independent experiments are shown. Student's t test (B, C, H, and K), two-way ANOVA and Sidak's posthoc test (D), or one-way ANOVA with Tukey's posthoc test (F, G, and I) were used. *, $P < 0.05$; **, $P < 0.01$; ***, $P < 0.001$; ****, $P < 0.0001$. All values are mean ± SEM.

Microglia lacking CR3 are more efficient in degrading extracellular Aβ

In the brain, CR3 is exclusively expressed on microglia, allowing us to interpret changes in Aβ deposition in the context of microglia-dependent mechanisms. To study these mechanisms in a myeloid cell model system, we generated a stable CR3 knockdown BV2 cell line (CR3^{kd}) and confirmed knockdown efficiency by Western blotting and flow cytometric analysis of CD11b expression (Fig. 2, A and B). First, we assessed the possibility that changes in phagocytosis are responsible for the decrease in plaque accumulation by measuring phagocytic activity of CR3^{kd} cells. In agreement with published data (Fu et al., 2012), we found a significant decrease in baseline phagocytosis (Fig. 2 C) and phagocytic efficiency (Fig. 2 D) in CR3-deficient cells.

BV2 cells secrete several enzymes capable of degrading extracellular Aβ (Qiu et al., 1997). We established an in vitro Aβ degradation assay (Fig. 2 E) by adding freshly solubilized Aβ42 to serum-free medium on control or CR3^{kd} cells and collecting the conditioned medium for ELISA measurements at different time points. Aβ was removed more rapidly from the supernatant of CR3^{kd} than control cells (Fig. 2 F). Interestingly, this effect was also present in a cell-free system where Aβ42 peptide was added to conditioned medium alone (Fig. 2 G). We confirmed these findings using cultured primary microglia isolated from adult WT and CR3$^{-/-}$ mice. CR3$^{-/-}$ microglia and their supernatant showed increased activity in the cell-based and the cell-free Aβ degradation assay compared with microglia from WT mice (Fig. 2, H and I).

To test in vivo whether degradation of exogenously added Aβ is enhanced in CR3$^{-/-}$ mice, we injected preaggregated Aβ42 stereotactically into the hippocampus of WT and CR3$^{-/-}$ animals and quantified residual Aβ immunoreactivity after 5 d. Aβ was removed more rapidly from the hippocampus of CR3$^{-/-}$ mice than WT mice (Fig. 2, J and K).

Collectively, our findings indicate that CR3-deficient microglia and microglia-like cells are more efficient in removing stereotactically injected Aβ in vivo and soluble Aβ in vitro, respectively.

CR3 deficiency results in increased secretion of Aβ-degrading enzymes

To determine whether proteases mediate the increase in Aβ-degrading activity, we added various protease inhibitors in the cell-free Aβ degradation assay (Fig. S1, A and B). Then, we evaluated how they affected the Aβ degradation ratio between conditioned supernatants of cultured primary adult microglia isolated from WT and CR3$^{-/-}$ mice. A complete protease inhibitor cocktail lacking EDTA and captopril, an angiotensin-converting enzyme inhibitor, had no effect on Aβ degradation (Fig. 3 A). However, several other inhibitors lessened the Aβ-degrading activity significantly. The neprilysin inhibitor thiorphan reduced the degrading activity slightly, suggesting some involvement of neprilysin. The most potent inhibitors were the complete protease inhibitor cocktail containing EDTA, EDTA itself, and PMSF, a serine protease inhibitor. EDTA is a strong inhibitor of metalloproteinases, and matrix metalloproteinase 2 (MMP2) and MMP9 have previously been implicated as major Aβ-degrading enzymes (Yan et al., 2006; Hernandez-Guillamon et al., 2010). MMPs are regulated on the transcriptional and activity level, leading us to quantify mRNA expression as well as protease activity. We found mRNA expression of MMP2 and 9, as well as of MMP8, 12, 13, and 14, unchanged between acutely isolated microglia from APP and APP/CR3$^{-/-}$ mice (Fig. 3 B and Fig. S1 G). We also measured MMP activity using assays for MMP2 and MMP9 activity, finding that overall MMP activity and activity of specific MMPs were not significantly changed in conditioned supernatant or cortical lysates from CR3$^{-/-}$ mice (Fig. S1, C–F).

The serine protease inhibitor PMSF also showed strong inhibition of the Aβ-degrading activity; one serine protease that has been implicated in Aβ degradation is tissue plasminogen activator (tPA), which degrades Aβ via plasminogen activation (Melchor et al., 2003). Mice lacking tPA or plasminogen are less efficient at degrading Aβ injected in the hippocampus (Melchor et al., 2003), but the function of tPA in microglia remains poorly understood (Tsirka et al., 1995; Gravanis and Tsirka, 2005). tPA mRNA levels were unchanged between acutely isolated primary adult microglia-like cells from APP and APP/CR3$^{-/-}$ mice (Fig. 3 C). However, active tPA protein levels were significantly higher in conditioned medium from CR3^{kd} than from control cells (Fig. 3 D). Tissue zymography, which measures proteolytic activity ex vivo in tissue sections and, in the central nervous system, predominantly detects tPA activity (Tsirka et al., 1995), revealed significantly higher activity in APP/CR3$^{-/-}$ than in APP mice (Fig. 3, E and F). Additionally, targeting tPA expression in CR3^{kd} cells by siRNA reduced the Aβ-degrading activity (Fig. 3 G) by decreasing tPA mRNA levels (Fig. 3 H).

Together, these data suggest that tPA, as well as an EDTA chelation-sensitive protease activity are responsible for the enhanced Aβ degradation by CR3-deficient cells and may account for the mechanism underlying the decreased Aβ deposition in vivo.

Targeting CR3 with the small molecule LA-1 results in increased Aβ degradation in vitro and reduced Aβ levels in vivo

Our data suggest that modulating CR3 could lead to enhanced Aβ clearance in the AD brain. Leukadherins are small molecule modulators of CR3 function that bind to its CD11b subunit, thereby increasing cell adhesion (Maiguel et al., 2011). We found that treatment of BV2 cells with LA-1 resulted in a concentration-dependent increase in Aβ degradation (Fig. 4 A). This effect was absent in CR3^{kd} cells (Fig. 4 B), confirming that LA-1 requires the presence of CR3. Consistent with these findings, young, preplaque APP mice treated for 10 d with daily i.p. injections of LA-1 had significantly reduced Aβ levels in the guanidine-extracted fractions of the cortex and a trend toward a reduction in the hippocampus compared with vehicle-treated mice (Fig. 4 C). LA-1 did not change APP expression and processing in a cell line, indicating that the drug reduces Aβ through other mechanisms (Fig. S2, A–F).

Mass spectrometry analysis of whole-brain lysates from mice treated with a single dose of LA-1 showed a spike in LA-1 concentration 15 min after injection with detectable levels of the drug at the 2-h time point, demonstrating BBB penetration (Fig. 4 D). Plasma levels also spiked at 15 min, but LA-1 was undetectable at 2 h after injection (Fig. S2 H). Flow cytometric analysis of acutely isolated microglia and PBMCs revealed no changes in vascular adhesion markers (Fig. S2, I and J).

Similar to microglia from CR3$^{-/-}$ mice, we did not observe differences in MMP2 or MMP9 mRNA levels in microglia from LA-1–treated mice (Fig. 4 F), nor in the expression of other MMPs (Fig. S2 G). However, we did find a significant increase in tPA mRNA (Fig. 4 E), suggesting that LA-1 may exert its function through tPA as well.

LA-1 treatment results in decreased ISF Aβ levels and decreased ISF Aβ half-life

To directly monitor whether LA-1 treatment increases soluble Aβ clearance, we used in vivo microdialysis, which allows measurement of soluble Aβ levels in the mouse ISF. We used APP/PS1-ΔExon9–transgenic mice (Jankowsky et al., 2004), which are routinely used for in vivo microdialysis (Yan et al., 2009; Cramer et al., 2012; Kraft et al., 2013) at an age before

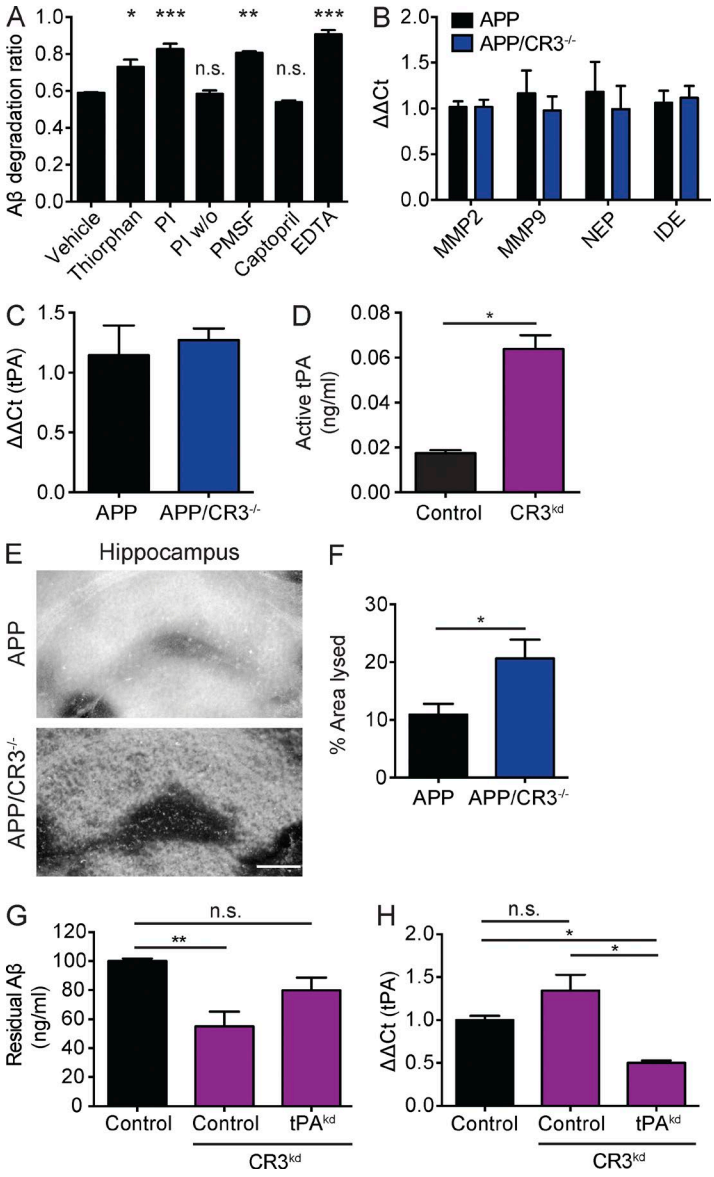

Figure 3. **CR3-deficient cells and mice display increased tPA activity.** (A) Ratio of Aβ measured in conditioned medium from CR3^{kd} versus control BV2 cells after addition of proteinase inhibitors. A representative graph of two independent experiments is shown. PI, protease inhibitor; PI w/o, protease inhibitor cocktail lacking EDTA. (B and C) qPCR analysis of mRNA from adult primary microglia, normalized to GAPDH. Microglia were from $n = 7$ individual mice. IDE, insulin-degrading enzyme; NEP, neprilysin. (D) Active tPA measurement in conditioned medium from control and CR3^{kd} cells. $n = 2$ independent experiments. (E and F) Representative image of in situ zymography in the hippocampus (E) and quantification of the lysed area (F). $n = 5$–6 mice. All mice were 3–4-mo-old males and females. Bar, 500 µm. (G) Aβ degradation assay in control and CR^{kd} cells transfected with control siRNA or tPA siRNA. (H) Knockdown efficiency was quantified by qPCR. Data are combined from two independent experiments. One-way ANOVA with Dunnett's posthoc test and significance relative to vehicle (A), unpaired Student's *t* test (B, C, D, and F), or one-way ANOVA with Tukey's posthoc test (G and H) were used. *, $P < 0.05$; **, $P < 0.01$; ***, $P < 0.001$. All values are mean ± SEM.

Aβ deposition. Reverse microdialysis of LA-1 into the hippocampus significantly reduced steady-state Aβ levels in the ISF (Fig. 5, A and B), consistent with our hypothesis. This effect is reversible, as exchanging the drug for standard perfusion buffer led to a rapid return to baseline steady-state Aβ levels (Fig. 5, D and E). To measure the half-life of Aβ, its production was stopped with the γ-secretase inhibitor Compound E, revealing that the rate of concentration decline was significantly reduced in LA-1–treated mice (Fig. 5 C). We then repeated these experiments using APP and APP/CR3$^{-/-}$ mice and found that mice lacking CR3 did not show a reduction in ISF Aβ levels below baseline after LA-1 treatment (Fig. 5, F and G). These results indicate that CR3 expression is necessary for LA-1–mediated enhancement of Aβ clearance. Collectively, these data suggest that modulating CR3 with LA-1 reduces brain Aβ levels by enhancing Aβ clearance from the ISF.

DISCUSSION

Despite advances in understanding the pathogenesis of AD, little is known about the events initiating the accumulation of Aβ in the brain and the contributions of the immune system. In recent years, several studies have focused on the role of microglia in the pathogenesis of AD. Although microglia are able to take up fibrillar Aβ into endosome-like compartments (Frackowiak et al., 1992; Meyer-Luehmann et al., 2008), they seem inefficient at degrading and removing Aβ deposits from the AD brain (Grathwohl et al., 2009). It has been suggested that the proinflammatory environment of the AD brain might make them less efficient phagocytes (Bamberger et al., 2003; Koenigsknecht-Talboo and Landreth, 2005). There is also evidence that microglia internalize and degrade soluble Aβ in lysosomes through fluid-phase macropinocytosis (Mandrekar et al., 2009) or through the secretion of various Aβ-degrading activities.

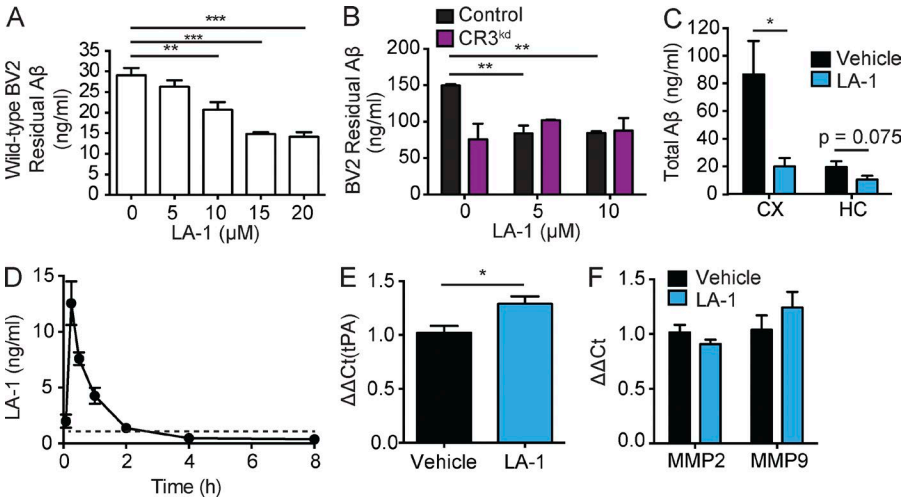

Figure 4. **The small molecule modulator LA-1 enhances Aβ degradation in vitro and lowers Aβ levels in vivo.** (A and B) Quantification of cell-based Aβ degradation assay with LA-1 treatment in BV2 cells (A) and LA-1 treatment in control and CR3^{kd} cell lines (B). Representative graphs of two to three experiments are shown. (C) Aβ levels in guanidine-extracted fraction in APP mice after LA-1 treatment. *n* = 8–9 mice, male and female. CX cortex, HC hippocampus. (D) Mass spectrometry quantification of brain levels of LA-1 after single injection. *n* = 3 per time point, all male mice. (E and F) qPCR analysis of mRNA from primary microglia. *n* = 5 individual mice, male and female. The dashed line shows the detection limit. (C–F) All mice were 3–4 mo old. One-way ANOVA and Tukey's posthoc test (A), two-way ANOVA and Bonferroni posthoc test (B), or unpaired Student's *t* test (C, E, and F) was used. *, P < 0.05; **, P < 0.01; ***, P < 0.001. All values are mean ± SEM.

Aβ degradation in the extracellular space can be accomplished by several enzymes, and published studies have mainly focused on the proteases neprilysin, insulysin (insulin-degrading enzyme), MMP2, MMP9, and tPA/plasmin (Iwata et al., 2001; Melchor et al., 2003; Song and Hersh, 2005; Eckman et al., 2006; Yan et al., 2006; Hernandez-Guillamon et al., 2010). Our inhibitor screen suggests that neprilysin plays a minor role in the increased Aβ degradation in our model, and quantitative PCR (qPCR) on mRNA isolated from primary adult microglia did not show changes in neprilysin or insulin-degrading enzyme expression. We did uncover an activity sensitive to EDTA chelation that is regulated by CR3, but quantification of MMP activity and mRNA of several MMPs failed to identify a specific isoform. It is possible that our methods were not sensitive enough to measure the specific MMP activity or that a different, as yet unidentified, EDTA-sensitive protease mediates this effect. However, we did find increased levels of active tPA in vitro and in vivo under CR3-deficient conditions. tPA has previously been described as part of an important Aβ degradation pathway (Melchor et al., 2003). It can activate both plasminogen and MMPs and, therefore, mediate Aβ degradation via different pathways (Hahn-Dantona et al., 1999; Ramos-DeSimone et al., 1999). Additionally, tPA can bind LRP1 and could mediate efflux of Aβ from the mouse brain by facilitating BBB transport (Su et al., 2008). The fact that we found increased levels of active tPA in vitro and in vivo identifies it as one of the likely mediators of enhanced Aβ degradation in APP/CR3$^{-/-}$ mice.

The small molecule LA-1 was originally identified through a screen searching for monocyte adhesion enhancers, and it has been suggested that it mediates its effects by changing the local conformation of the extracellular domain of CD11b (Maiguel et al., 2011; Faridi et al., 2013). It has been used to anchor CR3-expressing cells in place and prevent infiltration of proinflammatory monocytes after injury in peripheral organs (Maiguel et al., 2011; Jagarapu et al., 2015). However, the effects of LA-1 on microglia have not been studied. We found that LA-1 enhances extracellular Aβ degradation and that it can lower Aβ levels in vivo by enhancing clearance from the ISF. Furthermore, LA-1 treatment in mice results in increased levels of tPA mRNA in acutely isolated microglia.

In summary, both lack of CR3 and treatment with LA-1 lead to increased Aβ degradation in vitro, and LA-1 increases Aβ clearance in vivo. Furthermore, tPA activity was increased in conditioned media of CR3^{kd} cells and in APP/CR3$^{-/-}$ brain tissue, and tPA mRNA levels were increased in microglia isolated from LA-1–treated mice, suggesting at least in part a similar mechanism. To date, little is known about the effects of CR3 deficiency or LA-1 treatment in microglia relating to the secretory or expression profiles. There is evidence from studies in human PBMC–derived macrophages, human monocyte cell lines (Reed et al., 2013), and in human NK cells (Roberts et al., 2016) that LA-1 treatment can affect key transcription factors, e.g., MyD88, to modulate secretion of cytokines. LA-1 might act as a partial antagonist, reducing signaling that inhibits the secretion of Aβ-degrading enzymes, although leaving other functions unaffected or even enhancing them (e.g., adhesion). Thus, LA-1 might mimic CR3 deficiency in some aspects but not in all microglial functions and signaling pathways. Future studies will have to dissect how LA-1 engages CR3 and how CR3 modulation results in the release of an Aβ-degrading activity from microglia. Our data indicate a novel function of the phagocytic receptor CR3 in the suppression of microglia-mediated clearance of soluble Aβ. Furthermore, targeting CR3 with a small molecule can reduce Aβ levels in brains of APP-transgenic mice by

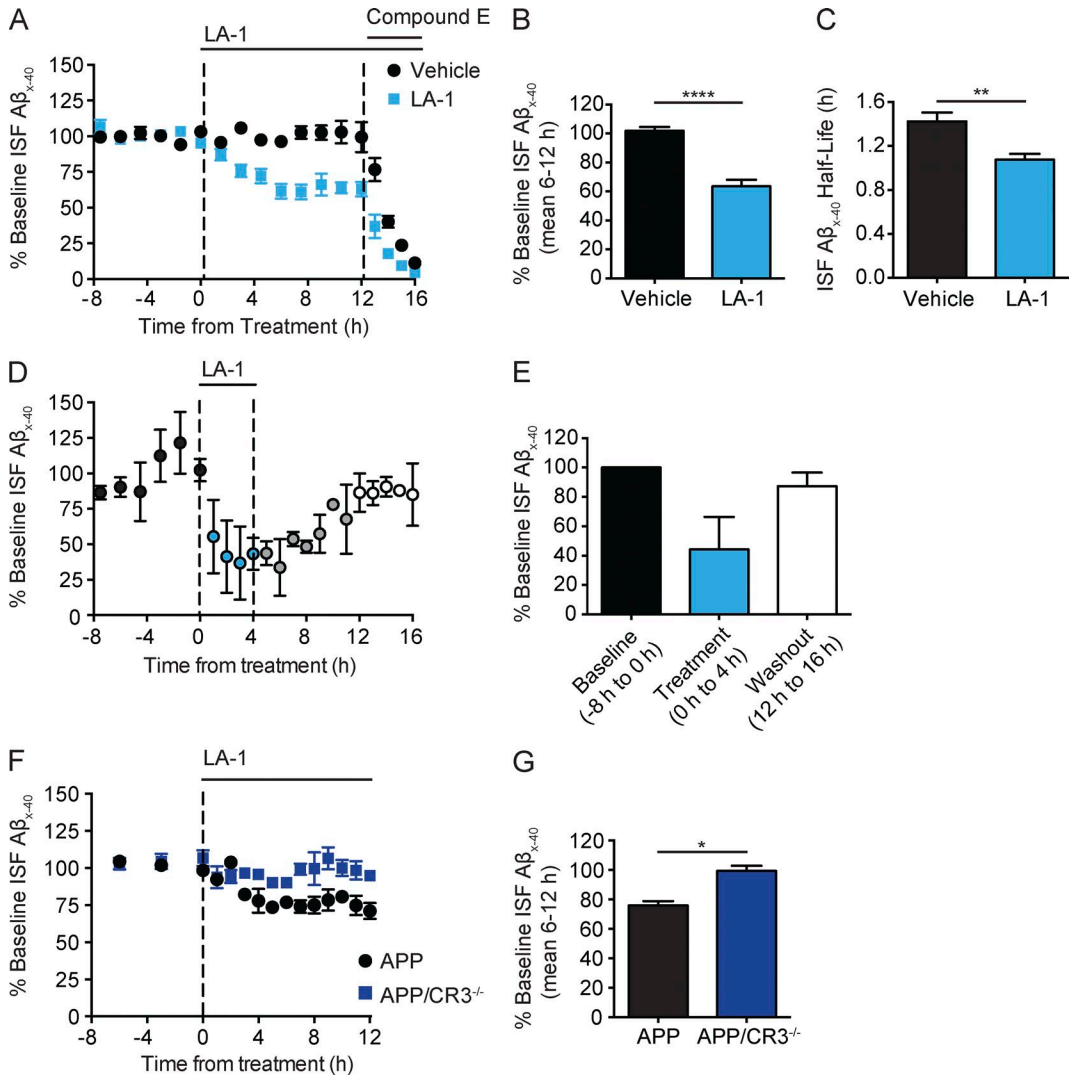

Figure 5. **LA-1 treatment decreases ISF Aβ concentration by enhancing clearance.** (A) Time course of in vivo microdialysis. 8 h of baseline measurements, followed by LA-1 infusion for 16 h, and the last 4 h with additional infusion of Compound E. (B) Quantification of ISF Aβ concentrations after 6 h of LA-1 infusion. (C) Quantification of Aβ half-life. (D) Time course of in vivo microdialysis. 8-h baseline measurements, followed by 4-h LA-1 infusion and 12-h washout. (E) Quantification of D. (F) Time course of in vivo microdialysis in APP and APP/CR3$^{-/-}$ mice with 8 h of baseline, followed by 12 h of LA-1 infusion. (G) Quantification of ISF Aβ concentration after 6 h of LA-1 infusion. $n = 5$ mice per group, male and female (A–C); $n = 2$ mice, all male (D and E); or APP, $n = 2$ and APP/CR3$^{-/-}$, $n = 5$, male and female (F and G). Unpaired Student's t test was used. *, $P < 0.05$; **, $P < 0.01$; ****, $P < 0.0001$. All values are mean ± SEM.

enhancing Aβ clearance from the extracellular space. Therefore, CR3 may be a potential therapeutic target for the treatment or prevention of AD.

MATERIALS AND METHODS

Transgenic mice

T41 APP-transgenic mice (mThy-1-*hAPP751*$_{V171I,KM670/671NL}$), CR3-deficient mice (*Itgam*$^{tm1Myd+/-}$), and *APP/PS1*$^{+/-}$ (mPrP-*hAPP*$_{KM670/671NL}$ *PS1-ΔExon9*) mice have been described previously (Soriano et al., 1999; Rockenstein et al., 2001; Savonenko et al., 2005). All lines were maintained on a C57BL/6 genetic background. All animal procedures were conducted with approval of the Animal Care and Use Committee of the Veterans Administration Palo Alto Health Care System.

Tissue collection and processing

Mice were anesthetized with 400 mg/kg chloral hydrate (Sigma-Aldrich) and transcardially perfused with sterile PBS. Brains were removed and divided saggitally. One hemibrain was postfixed in phosphate-buffered 4% paraformaldehyde, pH 7.4, at 4°C for 48 h, cryoprotected in 30% sucrose in PBS, and sectioned at 35 µm with a freezing microtome (Leica Biosystems). The other hemibrain was snap frozen and stored at −80°C for further analysis.

Immunohistochemistry and image analysis

Immunohistochemistry was performed on free-floating sections according to standard procedures. In brief, fixed sections were treated with 0.1% Triton X-100 and 0.6% hydrogen peroxide and blocked using an avidin and biotin blocking kit (Vector Laboratories), followed by incubation with biotinylated 3D6 (Perrigo Company) antibody at 1:8,000 overnight at 4°C. Primary antibody labeling was revealed using an ABC kit (Vector Laboratories) followed by diaminobenzedine staining (Sigma-Aldrich). For the transgenic animals, six sections separated by 480 µm were analyzed per animal. After stereotactic injections, brains were sectioned at 35 µm, and all sections surrounding the injection site were collected (a minimum of 10 sections to either side) and stained. Images were acquired using a NanoZoomer slide scanner (Hamamatsu Photonics), and immunoreactivity was quantified with ImageJ software (National Institutes of Health) in a blinded fashion with a fixed threshold for all sections. For the stereotactic injections, all immunoreactivity was added up and normalized to WT levels independently for two experiments.

Drug treatment

LA-1–treated mice were injected for 10 d, daily, i.p. with 500 µl of 50 µM LA-1 (EMD Millipore) or DMSO vehicle in PBS. For reverse microdialysis, drugs were diluted in microdialysis perfusion buffer. Compound E was purchased from Sigma-Aldrich. Cells were incubated with LA-1 in vitro at the indicated concentrations in serum-free culture medium for 3–6 h. For assessment of APP processing in APP-overexpressing Chinese hamster ovary cells (Weggen et al., 2003), lysates and supernatants were collected after 6 h.

Cell lines

BV2 cells were maintained in DMEM containing 10% FBS. CR3 knockdown ($CR3^{kd}$) cells were generated by transduction with a CD11b-targeting shRNA lentivirus carrying a puromycin resistance cassette (OriGene) or empty vector control virus. Stable lines were selected with 5 µg/ml puromycin. In addition to puromycin selection, knockdown cell lines were maintained by sorting of $CD11b^{low}$ cells from the mixed culture.

For siRNA-mediated transient knockdown, BV2 control and $CR3^{kd}$ cells were transiently transfected on day 1 using Viromer Blue reagent (Lipocalyx) and On-Target SMA RT-pool siRNA-targeting mouse *Plat* (tPA; GE Healthcare) expression and control siRNA (GE Healthcare) according to the manufacturer's instructions. After 48 h, cells were replated and used for the in vitro Aβ degradation assay. siRNA pool target sequences for Plat were: 5′-CGGCCUCAGUUUAGAAUUA-3′, 5′-GAAGCAGCCGGGUGGAAUA-3′, 5′-GAAAGCUGACGUGGGAAUA-3′, and 5′-AAAGUGGUCUUGGGCAGAA-3′. Sequences for the control siRNA were not provided by the manufacturer.

Isolation of primary adult mouse microglia

Adult microglia were isolated using a neural dissociation kit (Miltenyi Biotec) followed by magnetic-activated cell sorting with CD45 micro beads (Miltenyi Biotec) according to the manufacturer's instructions. CD45 antibody–coupled beads were used as a replacement for CD11b beads, as the receptor is lacking in the CR3-deficient animals. In brief, perfused brains of 3–4-mo-old mice were dissociated using the neuronal dissociation kit (Miltenyi Biotec), incubated with CD45 microbeads (Miltenyi Biotec), and separated using an LS separation column (Miltenyi Biotec). For functional studies, the cells were allowed to recover for 3 d in DMEM/F12 with 10% FBS. Cells for RNA were immediately frozen at −80°C. Cells used for flow cytometry were kept on ice and stained immediately.

In vivo microdialysis and quantitative measurement of ISF Aβ

In vivo microdialysis was performed as previously described (Cirrito et al., 2003; Castellano et al., 2011). In brief, microdialysis guide cannula and probes with a 38-kD molecular weight cutoff membrane (BR-2 probes; Bioanalytical Systems) were inserted into the left hippocampus at the following coordinates: bregma, −3.1 mm; midline, −2.5 mm; and tip, 3.2 mm below dura at a 12° angle. Perfusion buffer (0.15% BSA in artificial cerebrospinal fluid [in mM: 1.3 CaCl, 1.2 $MgSO_4$, 3 KCl, 0.4 KH_2PO_4, 25 $NaHCO_3$, and 122 NaCl, pH 7.35]) was perfused at a 1-µl/min flow rate with a syringe pump (Stoelting Co). Microdialysis samples were collected every 60–90 min using a refrigerated fraction collector (Univentor). Mice were housed in a RaTurn Caging system (Bioanalytical Systems) with ad libitum food and water for the duration of the experiment. LA-1 and Compound E (AsisChem) were perfused directly into the hippocampus through the microdialysis probe (reverse microdialysis) at a concentration of 100 µM and 200 nM, respectively.

Quantitative measurements of Aβ collected from in vivo microdialysis fractions were performed by sandwich ELISA, as previously described (Cirrito et al., 2011). ELISA plates were coated with a mouse anti-$Aβ_{40}$ selective antibody, mHJ2, and detected with a biotinylated central domain mouse anti-Aβ (amino acids 13–28) antibody, mHJ5.1.

Aβ degradation assay

For the cell-based degradation assay, BV2 cells or primary microglia were plated at 250,000 cells per well on 24-well plates and allowed to attach overnight. The next morning, the medium was exchanged for serum-free DMEM containing 1 µg/ml freshly solubilized Aβ1-42 peptide (Bachem). For treatment with LA-1 or vehicle, serum-free DMEM containing LA-1 or vehicle was added to the cells 30 min before Aβ1-42 was added at 1 µg/ml. For the cell-free assay, serum-free DMEM was conditioned for 16–18 h for BV2 cells and for 48 h for primary microglia at the same cell density. The supernatant was centrifuged at 1,000 *g* for 15 min to

remove cells and debris and transferred into a fresh tube. Aβ1-42 was added at 1 μg/ml to the conditioned supernatants and incubated. For both assays, samples were taken at defined time points and transferred into a tube containing complete protease inhibitor cocktail (Roche) to a final concentration of 2×.

Aβ ELISA and tissue preparation

ELISAs were performed using Meso Scale technology (Meso Scale Discovery). Multiarray 96-well plates (Meso Scale Discovery) were coated with capture antibody 21D12 for total Aβ (Aβ12-28; Elan Pharmaceuticals). Plates were washed, and diluted samples or Aβ1-40 peptide standards were added. Aβ was detected using biotinylated 3D6 antibody (Elan Pharmaceuticals) and SULFO-TAG streptavidin (Meso Scale Discovery). Plates were read on a Sector Imager 2400 (Meso Scale Discovery), and samples were normalized to Aβ standards.

Mouse tissue was subjected to serial Aβ extraction using PBS, RIPA (50 mM Tris-HCl, pH 7.4, 150 mM sodium chloride, 1% Nonidet P40, 1 mM EDTA, and 0.25 deoxycholic acid), and guanidine buffer (5 M guanidine-HCl in 50 mM Tris-HCl), with all buffers containing complete protease inhibitor cocktail (Roche) at a concentration of 2×.

Gelatinase and MMP activity assays

Activity of gelatinase and MMPs was measured using the EnzCheck Gelatinase/Collagenase Assay kit (Thermo Fisher Scientific) and the SensoLyte 520 Generic MMP Assay kit and SensoLyte 520 MMP Profiling kit (AnaSpec) according to the manufacturers' instructions. A list of the MMP-specific fluorescence resonance energy transfer substrates used in the MMP Profiling kit can be found in Table S2. Cell culture supernatants for the gelatinase/collagenase assay were conditioned for 24 h in phenol red–free DMEM and stored at −80°C until use. The MMP assays were performed with 50 μg mouse brain lysate per well.

tPA zymography and active tPA measurements

Hippocampal tPA activity was measured by in situ zymography with casein substrate, as previously described (Sachs et al., 2007). In brief, fresh frozen, Tissue-TEK optimal cutting temperature (Sakura)–embedded brains were sections at 12 μm, and sections 120 μm apart were used. The sections were overlaid with substrate, and the area lysed was quantified. tPA activity in conditioned cell culture medium was measured using the active mouse tPA functional assay ELISA kit (Molecular Innovations) according to the manufacturer's instructions.

Phagocytosis assay

BV2 cells were plated on 24-well plates at a density of 50,000 cells per well in DMEM with 10% FBS. Cells were allowed to settle on the plate for 1–2 h in a tissue culture incubator. Fluorescent carboxyl microspheres (6 μm, flash red; Bangs Laboratories Inc.) were opsonized for 30 min in 50% FBS and PBS and then added to the BV2 cells at a concentration of 10 beads per cell. Cells and beads were incubated for 1 h in the tissue culture incubator and subsequently transferred to 5 ml polystyrene FACS tubes with the aid of TrypLE Express reagent (Thermo Fisher Scientific). Cells were washed twice with cold FACS buffer (1% FBS and 0.02% sodium azide in PBS) and then analyzed by flow cytometry.

RNA extraction and real-time PCR

RNA was extracted using the RNeasy kit (QIAGEN) according to the manufacturer's instructions. 100 ng of extracted microglial mRNA was reverse transcribed using the SuperScript III first strand synthesis system (Thermo Fisher Scientific). Gene expression was assessed using intron-spanning primers (for sequences, see Table S1), and GAPDH was used as the housekeeping gene. 1:20 diluted cDNAs were mixed with the probes and 2× LightCycler 480 SYBR Green I Master mix (Roche) and amplified using a Roche Light Cycler 480 (Roche). Results were analyzed using the ΔΔCt method.

Western blotting

Tissue or cells were lysed on ice in RIPA buffer (50 mM Tris-HCl, pH 7.4, 150 mM sodium chloride, 1% Nonidet P40, 1 mM EDTA, and 0.25 deoxycholic acid) with complete protease inhibitor (Roche), and the total protein concentration was measured using a bicinchoninic assay kit (Thermo Fisher Scientific). Lysates were run on 4–12% Bis-Tris gels (Thermo Fisher Scientific) in 1× NuPage MES SDS running buffer (Thermo Fisher Scientific). Proteins were transferred overnight onto nitrocellulose membranes in 20% (vol/vol) methanol in NuPage Transfer buffer (Thermo Fisher Scientific). Membranes were blocked and then incubated in primary antibody overnight. Proteins were visualized and quantified on an Odyssey infrared imaging system (LI-COR Biosciences). The following antibodies were used: CT15 (Sisodia et al., 1993), β-actin (Sigma-Aldrich), neuron-specific enolase (5E2; Thermo Fisher Scientific), and IC16 (Hahn et al., 2011).

Mass spectrometric analysis of LA-1 in brain and plasma

C57BL/6 mice were injected i.p. with 500 μl of 50 μM LA-1. At seven time points after injection (5 min, 15 min, 30 min, 1 h, 2 h, 4 h, and 8 h), mice were anesthetized, and EDTA blood was collected by cardiac puncture. After blood collection, the mice were perfused with sterile PBS, and the brain was collected and immediately frozen as hemibrains at −80°C. Plasma was isolated from whole blood immediately by spinning at 1,000 *g* and stored at −80°C. Three animals were used per time point. Right hemibrains were homogenized in 2 volumes of deionized water, using one volume of 0.5-mm glass beads (Next Advance) in a Bullet Blender (Next Advance). Brain homogenates and plasma samples were further diluted in 50% and 20% methanol in acetonitrile. Samples were mixed and clarified by centrifugation before analysis on a mass spectrometer (Qtrap 4000; Sciex). 10 μl of each sample was introduced into the mass spectrometer via a Dionex microcapillary column (C18 5 μm 2.1 × 100 mm; Thermo Fisher Scientific). Samples were eluted via 300 μl/min isocratic flow of 85%

B (mobile phase A: 0.1 mM ammonium acetate in water; mobile phase B: 100% acetonitrile) for 2 min. Quantification of LA-1 was performed using multiple reaction monitoring transitions m/z 420.103-375.800 and m/z 420.103-230.000. Method development, data acquisition, and data processing were performed using Analyst 1.6.1 software (Sciex). LA-1 was quantified using untreated brain homogenates with spiked-in LA-1 standards, and standard curves were generated using cubic regression. Unknown LA-1 concentrations were interpolated from the brain homogenate and plasma standard curves using Prism 6 analysis software (GraphPad Software).

Stereotactic injection of Aβ

For stereotactic injection of Aβ, the mice were anesthetized to full muscle relaxation with isoflurane (2.5–3.5% with oxygen, to effect) and placed in a stereotaxic device. Surgeries were performed on heated pads, and body temperature was monitored throughout the procedure. The skull was exposed, and a hole was drilled into the skull at the injection site (coordinates from bregma: A = −2 mm and L = −1.8 mm; from brain surface: H = −2 mm) to target the hippocampus. A microsyringe (25 G) was used to infuse 1 µg of Aβ into the brain over 2 min. The cannula was left in place for an additional 3 min and slowly withdrawn. The incision in the scalp was closed, and the animals were allowed to recover. The animals received 0.05–0.1 µg/ml buprenorphine as directed for pain.

Flow cytometry and FACS

Flow cytometric analysis was performed on a Fortessa or FACSCalibur FACS machine (BD). Standard staining was performed. In brief, cells were washed three times with FACS buffer and blocked using Fc-block CD16/32 antibody (BioLegend) for 15 min, followed by incubation with fluorescently labeled antibody for 30 min. Analysis was performed using FlowJo software (version 9.2; Tree Star). PBMCs were isolated by Ficoll centrifugation. The antibodies used were: CD11b-PE antibody (BioLegend), CD162–Alexa Fluor 647 (BD), CD62L-FITC and CD18-PE (eBioscience), and CD54-APC, CD14-Pe/Cy7, CD49d-FITC, CD11a-PE, CD11b–eFluor 450 (all BioLegend). Sterile FACS to maintain CD11b knockdown in $CD11b^{kd}$ BV2 cell lines was performed after staining of $CR3^{kd}$ and control cells with CD11b-PE antibody, as described in the previous paragraph. Cells were sorted on a FACSAriaIII cell sorter (BD) for $CD11b^{low}$-expressing cells, defined by CD11b expression of <80% of control cells. Then, cells were cultured as described in the Cell lines section.

Online supplemental material

Fig. S1 shows that MMP activity and expression is not changed in CR3-deficient cells or mice. Fig. S2 shows that LA-1 does not affect APP processing and does not change the expression of vascular adhesion markers on PBMCs or microglia. Table S1 contains the qPCR primer sequences, and Table S2 shows the sequences of fluorescence resonance energy transfer substrates used in the MMP activity assays.

ACKNOWLEDGMENTS

The authors thank Dr. Daniela Berdnik for critical review of the manuscript, Dr. Zhaoqing Ding and Dr. Lusijah Roth for assistance with flow cytometry and FACS, Dr. Hui Zhang for maintaining APP transgenic mice, The Stanford Gene Vector and Virus Core (supported by National Institute of Neurological Disorders and Stroke grant no. P30 NS079375-01A1) for producing the lentiviruses used in this study, and Shaun T. Hund for general support.

Funding for this study was provided by the Alexander von Humboldt Foundation (E. Czirr), a Kirschstein National Research Service Award predoctoral fellowship (K.I. Mosher), the Jane Coffin Childs Memorial Fund for Medical Research (J.M. Castellano), the John Douglas French Alzheimer's Foundation (K.M. Lucin), National Institute of Neurological Disorders and Stroke (grant R35 NS097976 to K. Akassoglou), the National Institutes of Health/National Institute on Aging (grant R01 AG042513 to J.R. Cirrito), National Institutes of Health/National Institute of Neurological Disorders and Stroke (grant P01 NS074969 J.R. Cirrito), the Paul F. Glenn Center for the Biology of Aging (T. Wyss-Coray), the Department of Veterans Affairs (T. Wyss-Coray), and the National Institute on Aging (grant AG045034 to T. Wyss-Coray).

The authors declare no competing financial interests.

Submitted: 30 November 2016

Revised: 31 January 2017

Accepted: 3 February 2017

REFERENCES

Afagh, A., B.J. Cummings, D.H. Cribbs, C.W. Cotman, and A.J. Tenner. 1996. Localization and cell association of C1q in Alzheimer's disease brain. *Exp. Neurol.* 138:22–32. http://dx.doi.org/10.1006/exnr.1996.0043

Bamberger, M.E., M.E. Harris, D.R. McDonald, J. Husemann, and G.E. Landreth. 2003. A cell surface receptor complex for fibrillar β-amyloid mediates microglial activation. *J. Neurosci.* 23:2665–2674.

Bardehle, S., V.A. Rafalski, and K. Akassoglou. 2015. Breaking boundaries—coagulation and fibrinolysis at the neurovascular interface. *Front. Cell. Neurosci.* 9:354. http://dx.doi.org/10.3389/fncel.2015.00354

Bateman, R.J., L.Y. Munsell, J.C. Morris, R. Swarm, K.E. Yarasheski, and D.M. Holtzman. 2006. Human amyloid-β synthesis and clearance rates as measured in cerebrospinal fluid in vivo. *Nat. Med.* 12:856–861. http://dx.doi.org/10.1038/nm1438

Castellano, J.M., J. Kim, F.R. Stewart, H. Jiang, R.B. DeMattos, B.W. Patterson, A.M. Fagan, J.C. Morris, K.G. Mawuenyega, C. Cruchaga, et al. 2011. Human apoE isoforms differentially regulate brain amyloid-β peptide clearance. *Sci. Transl. Med.* 3:89ra57. http://dx.doi.org/10.1126/scitranslmed.3002156

Cirrito, J.R., P.C. May, M.A. O'Dell, J.W. Taylor, M. Parsadanian, J.W. Cramer, J.E. Audia, J.S. Nissen, K.R. Bales, S.M. Paul, et al. 2003. In vivo assessment of brain interstitial fluid with microdialysis reveals plaque-associated changes in amyloid-β metabolism and half-life. *J. Neurosci.* 23:8844–8853.

Cirrito, J.R., B.M. Disabato, J.L. Restivo, D.K. Verges, W.D. Goebel, A. Sathyan, D. Hayreh, G. D'Angelo, T. Benzinger, H. Yoon, et al. 2011. Serotonin signaling is associated with lower amyloid-β levels and plaques in transgenic mice and humans. *Proc. Natl. Acad. Sci. USA.* 108:14968–14973. http://dx.doi.org/10.1073/pnas.1107411108

Cramer, P.E., J.R. Cirrito, D.W. Wesson, C.Y. Lee, J.C. Karlo, A.E. Zinn, B.T. Casali, J.L. Restivo, W.D. Goebel, M.J. James, et al. 2012. ApoE-directed therapeutics rapidly clear β-amyloid and reverse deficits in AD mouse models. *Science.* 335:1503–1506. http://dx.doi.org/10.1126/science.1217697

Czirr, E., and T. Wyss-Coray. 2012. The immunology of neurodegeneration. *J. Clin. Invest.* 122:1156–1163. http://dx.doi.org/10.1172/JCI58656

Daborg, J., U. Andreasson, M. Pekna, R. Lautner, E. Hanse, L. Minthon, K. Blennow, O. Hansson, and H. Zetterberg. 2012. Cerebrospinal fluid levels of complement proteins C3, C4 and CR1 in Alzheimer's disease.

J. Neural Transm. (Vienna). 119:789–797. http://dx.doi.org/10.1007/s00702-012-0797-8

Eckman, E.A., S.K. Adams, F.J. Troendle, B.A. Stodola, M.A. Kahn, A.H. Fauq, H.D. Xiao, K.E. Bernstein, and C.B. Eckman. 2006. Regulation of steady-state β-amyloid levels in the brain by neprilysin and endothelin-converting enzyme but not angiotensin-converting enzyme. *J. Biol. Chem.* 281:30471–30478. http://dx.doi.org/10.1074/jbc.M605827200

Ehlers, M.R. 2000. CR3: a general purpose adhesion-recognition receptor essential for innate immunity. *Microbes Infect.* 2:289–294. http://dx.doi.org/10.1016/S1286-4579(00)00299-9

Faridi, M.H., M.M. Altintas, C. Gomez, J.C. Duque, R.I. Vazquez-Padron, and V. Gupta. 2013. Small molecule agonists of integrin CD11b/CD18 do not induce global conformational changes and are significantly better than activating antibodies in reducing vascular injury. *Biochim. Biophys. Acta.* 1830:3696–3710. http://dx.doi.org/10.1016/j.bbagen.2013.02.018

Frackowiak, J., H.M. Wisniewski, J. Wegiel, G.S. Merz, K. Iqbal, and K.C. Wang. 1992. Ultrastructure of the microglia that phagocytose amyloid and the microglia that produce β-amyloid fibrils. *Acta Neuropathol.* 84:225–233. http://dx.doi.org/10.1007/BF00227813

Fu, H., B. Liu, J.L. Frost, S. Hong, M. Jin, B. Ostaszewski, G.M. Shankar, I.M. Costantino, M.C. Carroll, T.N. Mayadas, and C.A. Lemere. 2012. Complement component C3 and complement receptor type 3 contribute to the phagocytosis and clearance of fibrillar Aβ by microglia. *Glia.* 60:993–1003. http://dx.doi.org/10.1002/glia.22331

Grathwohl, S.A., R.E. Kälin, T. Bolmont, S. Prokop, G. Winkelmann, S.A. Kaeser, J. Odenthal, R. Radde, T. Eldh, S. Gandy, et al. 2009. Formation and maintenance of Alzheimer's disease β-amyloid plaques in the absence of microglia. *Nat. Neurosci.* 12:1361–1363. http://dx.doi.org/10.1038/nn.2432

Gravanis, I., and S.E. Tsirka. 2005. Tissue plasminogen activator and glial function. *Glia.* 49:177–183. http://dx.doi.org/10.1002/glia.20115

Guerreiro, R., A. Wojtas, J. Bras, M. Carrasquillo, E. Rogaeva, E. Majounie, C. Cruchaga, C. Sassi, J.S. Kauwe, S. Younkin, et al. Alzheimer Genetic Analysis Group. 2013. *TREM2* variants in Alzheimer's disease. *N. Engl. J. Med.* 368:117–127. http://dx.doi.org/10.1056/NEJMoa1211851

Hahn, S., T. Brüning, J. Ness, E. Czirr, S. Baches, H. Gijsen, C. Korth, C.U. Pietrzik, B. Bulic, and S. Weggen. 2011. Presenilin-1 but not amyloid precursor protein mutations present in mouse models of Alzheimer's disease attenuate the response of cultured cells to γ-secretase modulators regardless of their potency and structure. *J. Neurochem.* 116:385–395. http://dx.doi.org/10.1111/j.1471-4159.2010.07118.x

Hahn-Dantona, E., N. Ramos-DeSimone, J. Sipley, H. Nagase, D.L. French, and J.P. Quigley. 1999. Activation of proMMP-9 by a plasmin/MMP-3 cascade in a tumor cell model. Regulation by tissue inhibitors of metalloproteinases. *Ann. N.Y. Acad. Sci.* 878:372–387. http://dx.doi.org/10.1111/j.1749-6632.1999.tb07696.x

Hardy, J., and D.J. Selkoe. 2002. The amyloid hypothesis of Alzheimer's disease: progress and problems on the road to therapeutics. *Science.* 297:353–356. http://dx.doi.org/10.1126/science.1072994

Hernandez-Guillamon, M., S. Mawhirt, S. Fossati, S. Blais, M. Pares, A. Penalba, M. Boada, P.O. Couraud, T.A. Neubert, J. Montaner, et al. 2010. Matrix metalloproteinase 2 (MMP-2) degrades soluble vasculotropic amyloid-β E22Q and L34V mutants, delaying their toxicity for human brain microvascular endothelial cells. *J. Biol. Chem.* 285:27144–27158. http://dx.doi.org/10.1074/jbc.M110.135228

Hong, S., V.F. Beja-Glasser, B.M. Nfonoyim, A. Frouin, S. Li, S. Ramakrishnan, K.M. Merry, Q. Shi, A. Rosenthal, B.A. Barres, et al. 2016. Complement and microglia mediate early synapse loss in Alzheimer mouse models. *Science.* 352:712–716. http://dx.doi.org/10.1126/science.aad8373

Ivashkiv, L.B. 2009. Cross-regulation of signaling by ITAM-associated receptors. *Nat. Immunol.* 10:340–347. http://dx.doi.org/10.1038/ni.1706

Iwata, N., S. Tsubuki, Y. Takaki, K. Shirotani, B. Lu, N.P. Gerard, C. Gerard, E. Hama, H.J. Lee, and T.C. Saido. 2001. Metabolic regulation of brain Aβ by neprilysin. *Science.* 292:1550–1552. http://dx.doi.org/10.1126/science.1059946

Jagarapu, J., J. Kelchtermans, M. Rong, S. Chen, D. Hehre, S. Hummler, M.H. Faridi, V. Gupta, and S. Wu. 2015. Efficacy of leukadherin-1 in the prevention of hyperoxia-induced lung injury in neonatal rats. *Am. J. Respir. Cell Mol. Biol.* 53:793–801. http://dx.doi.org/10.1165/rcmb.2014-0422OC

Jankowsky, J.L., D.J. Fadale, J. Anderson, G.M. Xu, V. Gonzales, N.A. Jenkins, N.G. Copeland, M.K. Lee, L.H. Younkin, S.L. Wagner, et al. 2004. Mutant presenilins specifically elevate the levels of the 42 residue β-amyloid peptide in vivo: evidence for augmentation of a 42-specific γ secretase. *Hum. Mol. Genet.* 13:159–170. http://dx.doi.org/10.1093/hmg/ddh019

Jonsson, T., H. Stefansson, S. Steinberg, I. Jonsdottir, P.V. Jonsson, J. Snaedal, S. Bjornsson, J. Huttenlocher, A.I. Levey, J.J. Lah, et al. 2013. Variant of TREM2 associated with the risk of Alzheimer's disease. *N. Engl. J. Med.* 368:107–116. http://dx.doi.org/10.1056/NEJMoa1211103

Jun, G., A.C. Naj, G.W. Beecham, L.S. Wang, J. Buros, P.J. Gallins, J.D. Buxbaum, N. Ertekin-Taner, M.D. Fallin, R. Friedland, et al. Alzheimer's Disease Genetics Consortium. 2010. Meta-analysis confirms CR1, CLU, and PICALM as alzheimer disease risk loci and reveals interactions with APOE genotypes. *Arch. Neurol.* 67:1473–1484. http://dx.doi.org/10.1001/archneurol.2010.201

Koenigsknecht-Talboo, J., and G.E. Landreth. 2005. Microglial phagocytosis induced by fibrillar β-amyloid and IgGs are differentially regulated by proinflammatory cytokines. *J. Neurosci.* 25:8240–8249. http://dx.doi.org/10.1523/JNEUROSCI.1808-05.2005

Kraft, A.W., X. Hu, H. Yoon, P. Yan, Q. Xiao, Y. Wang, S.C. Gil, J. Brown, U. Wilhelmsson, J.L. Restivo, et al. 2013. Attenuating astrocyte activation accelerates plaque pathogenesis in APP/PS1 mice. *FASEB J.* 27:187–198. http://dx.doi.org/10.1096/fj.12-208660

Lambert, J.C., S. Heath, G. Even, D. Campion, K. Sleegers, M. Hiltunen, O. Combarros, D. Zelenika, M.J. Bullido, B. Tavernier, et al. European Alzheimer's Disease Initiative Investigators. 2009. Genome-wide association study identifies variants at CLU and CR1 associated with Alzheimer's disease. *Nat. Genet.* 41:1094–1099. http://dx.doi.org/10.1038/ng.439

Linnartz, B., and H. Neumann. 2013. Microglial activatory (immunoreceptor tyrosine-based activation motif)- and inhibitory (immunoreceptor tyrosine-based inhibition motif)-signaling receptors for recognition of the neuronal glycocalyx. *Glia.* 61:37–46. http://dx.doi.org/10.1002/glia.22359

Lucin, K.M., and T. Wyss-Coray. 2009. Immune activation in brain aging and neurodegeneration: too much or too little? *Neuron.* 64:110–122. http://dx.doi.org/10.1016/j.neuron.2009.08.039

Maier, M., Y. Peng, L. Jiang, T.J. Seabrook, M.C. Carroll, and C.A. Lemere. 2008. Complement C3 deficiency leads to accelerated amyloid β plaque deposition and neurodegeneration and modulation of the microglia/macrophage phenotype in amyloid precursor protein transgenic mice. *J. Neurosci.* 28:6333–6341. http://dx.doi.org/10.1523/JNEUROSCI.0829-08.2008

Maiguel, D., M.H. Faridi, C. Wei, Y. Kuwano, K.M. Balla, D. Hernandez, C.J. Barth, G. Lugo, M. Donnelly, A. Nayer, et al. 2011. Small molecule–mediated activation of the integrin CD11b/CD18 reduces inflammatory disease. *Sci. Signal.* 4:ra57. http://dx.doi.org/10.1126/scisignal.2001811

Mandrekar, S., Q. Jiang, C.Y. Lee, J. Koenigsknecht-Talboo, D.M. Holtzman, and G.E. Landreth. 2009. Microglia mediate the clearance of soluble Aβ through fluid phase macropinocytosis. *J. Neurosci.* 29:4252–4262. http://dx.doi.org/10.1523/JNEUROSCI.5572-08.2009

Melchor, J.P., R. Pawlak, and S. Strickland. 2003. The tissue plasminogen activator-plasminogen proteolytic cascade accelerates amyloid-β (Aβ)

degradation and inhibits Aβ-induced neurodegeneration. *J. Neurosci.* 23:8867–8871.

Meyer-Luehmann, M., T.L. Spires-Jones, C. Prada, M. Garcia-Alloza, A. de Calignon, A. Rozkalne, J. Koenigsknecht-Talboo, D.M. Holtzman, B.J. Bacskai, and B.T. Hyman. 2008. Rapid appearance and local toxicity of amyloid-β plaques in a mouse model of Alzheimer's disease. *Nature.* 451:720–724. http://dx.doi.org/10.1038/nature06616

Naj, A.C., G. Jun, G.W. Beecham, L.S. Wang, B.N. Vardarajan, J. Buros, P.J. Gallins, J.D. Buxbaum, G.P. Jarvik, P.K. Crane, et al. 2011. Common variants at MS4A4/MS4A6E, CD2AP, CD33 and EPHA1 are associated with late-onset Alzheimer's disease. *Nat. Genet.* 43:436–441. http://dx.doi.org/10.1038/ng.801

Qiu, W.Q., Z. Ye, D. Kholodenko, P. Seubert, and D.J. Selkoe. 1997. Degradation of amyloid β-protein by a metalloprotease secreted by microglia and other neural and non-neural cells. *J. Biol. Chem.* 272:6641–6646. http://dx.doi.org/10.1074/jbc.272.10.6641

Ramos-DeSimone, N., E. Hahn-Dantona, J. Sipley, H. Nagase, D.L. French, and J.P. Quigley. 1999. Activation of matrix metalloproteinase-9 (MMP-9) via a converging plasmin/stromelysin-1 cascade enhances tumor cell invasion. *J. Biol. Chem.* 274:13066–13076. http://dx.doi.org/10.1074/jbc.274.19.13066

Ray, S., M. Britschgi, C. Herbert, Y. Takeda-Uchimura, A. Boxer, K. Blennow, L.F. Friedman, D.R. Galasko, M. Jutel, A. Karydas, et al. 2007. Classification and prediction of clinical Alzheimer's diagnosis based on plasma signaling proteins. *Nat. Med.* 13:1359–1362. http://dx.doi.org/10.1038/nm1653

Reed, J.H., M. Jain, K. Lee, E.R. Kandimalla, M.H. Faridi, J.P. Buyon, V. Gupta, and R.M. Clancy. 2013. Complement receptor 3 influences toll-like receptor 7/8-dependent inflammation: implications for autoimmune diseases characterized by antibody reactivity to ribonucleoproteins. *J. Biol. Chem.* 288:9077–9083. http://dx.doi.org/10.1074/jbc.M112.403303

Roberts, A.L., B.G. Fürnrohr, T.J. Vyse, and B. Rhodes. 2016. The complement receptor 3 (CD11b/CD18) agonist Leukadherin-1 suppresses human innate inflammatory signalling. *Clin. Exp. Immunol.* 185:361–371. http://dx.doi.org/10.1111/cei.12803

Roberts, K.F., D.L. Elbert, T.P. Kasten, B.W. Patterson, W.C. Sigurdson, R.E. Connors, V. Ovod, L.Y. Munsell, K.G. Mawuenyega, M.M. Miller-Thomas, et al. 2014. Amyloid-β efflux from the central nervous system into the plasma. *Ann. Neurol.* 76:837–844. http://dx.doi.org/10.1002/ana.24270

Rockenstein, E., M. Mallory, M. Mante, A. Sisk, and E. Masliaha. 2001. Early formation of mature amyloid-β protein deposits in a mutant APP transgenic model depends on levels of $A\beta_{1-42}$. *J. Neurosci. Res.* 66:573–582. http://dx.doi.org/10.1002/jnr.1247

Ryu, J.K., and J.G. McLarnon. 2009. A leaky blood-brain barrier, fibrinogen infiltration and microglial reactivity in inflamed Alzheimer's disease brain. *J. Cell. Mol. Med.* 13:2911–2925. http://dx.doi.org/10.1111/j.1582-4934.2008.00434.x

Sachs, B.D., G.S. Baillie, J.R. McCall, M.A. Passino, C. Schachtrup, D.A. Wallace, A.J. Dunlop, K.F. MacKenzie, E. Klussmann, M.J. Lynch, et al. 2007. p75 neurotrophin receptor regulates tissue fibrosis through inhibition of plasminogen activation via a PDE4/cAMP/PKA pathway. *J. Cell Biol.* 177:1119–1132. http://dx.doi.org/10.1083/jcb.200701040

Saijo, K., and C.K. Glass. 2011. Microglial cell origin and phenotypes in health and disease. *Nat. Rev. Immunol.* 11:775–787. http://dx.doi.org/10.1038/nri3086

Savonenko, A., G.M. Xu, T. Melnikova, J.L. Morton, V. Gonzales, M.P. Wong, D.L. Price, F. Tang, A.L. Markowska, and D.R. Borchelt. 2005. Episodic-like memory deficits in the APPswe/PS1dE9 mouse model of Alzheimer's disease: relationships to β-amyloid deposition and neurotransmitter abnormalities. *Neurobiol. Dis.* 18:602–617. http://dx.doi.org/10.1016/j.nbd.2004.10.022

Schafer, D.P., E.K. Lehrman, A.G. Kautzman, R. Koyama, A.R. Mardinly, R. Yamasaki, R.M. Ransohoff, M.E. Greenberg, B.A. Barres, and B. Stevens. 2012. Microglia sculpt postnatal neural circuits in an activity and complement-dependent manner. *Neuron.* 74:691–705. http://dx.doi.org/10.1016/j.neuron.2012.03.026

Shen, Y., L. Lue, L. Yang, A. Roher, Y. Kuo, R. Strohmeyer, W.J. Goux, V. Lee, G.V. Johnson, S.D. Webster, et al. 2001. Complement activation by neurofibrillary tangles in Alzheimer's disease. *Neurosci. Lett.* 305:165–168. http://dx.doi.org/10.1016/S0304-3940(01)01842-0

Sisodia, S.S., E.H. Koo, P.N. Hoffman, G. Perry, and D.L. Price. 1993. Identification and transport of full-length amyloid precursor proteins in rat peripheral nervous system. *J. Neurosci.* 13:3136–3142.

Song, E.S., and L.B. Hersh. 2005. Insulysin: an allosteric enzyme as a target for Alzheimer's disease. *J. Mol. Neurosci.* 25:201–206. http://dx.doi.org/10.1385/JMN:25:3:201

Soriano, S.G., A. Coxon, Y.F. Wang, M.P. Frosch, S.A. Lipton, P.R. Hickey, and T.N. Mayadas. 1999. Mice deficient in Mac-1 (CD11b/CD18) are less susceptible to cerebral ischemia/reperfusion injury. *Stroke.* 30:134–139. http://dx.doi.org/10.1161/01.STR.30.1.134

Stevens, B., N.J. Allen, L.E. Vazquez, G.R. Howell, K.S. Christopherson, N. Nouri, K.D. Micheva, A.K. Mehalow, A.D. Huberman, B. Stafford, et al. 2007. The classical complement cascade mediates CNS synapse elimination. *Cell.* 131:1164–1178. http://dx.doi.org/10.1016/j.cell.2007.10.036

Su, E.J., L. Fredriksson, M. Geyer, E. Folestad, J. Cale, J. Andrae, Y. Gao, K. Pietras, K. Mann, M. Yepes, et al. 2008. Activation of PDGF-CC by tissue plasminogen activator impairs blood-brain barrier integrity during ischemic stroke. *Nat. Med.* 14:731–737. http://dx.doi.org/10.1038/nm1787

Tsirka, S.E., A. Gualandris, D.G. Amaral, and S. Strickland. 1995. Excitotoxin-induced neuronal degeneration and seizure are mediated by tissue plasminogen activator. *Nature.* 377:340–344. http://dx.doi.org/10.1038/377340a0

van Oijen, M., J.C. Witteman, A. Hofman, P.J. Koudstaal, and M.M. Breteler. 2005. Fibrinogen is associated with an increased risk of Alzheimer disease and vascular dementia. *Stroke.* 36:2637–2641. http://dx.doi.org/10.1161/01.STR.0000189721.31432.26

Weggen, S., J.L. Eriksen, S.A. Sagi, C.U. Pietrzik, V. Ozols, A. Fauq, T.E. Golde, and E.H. Koo. 2003. Evidence that nonsteroidal anti-inflammatory drugs decrease amyloid β42 production by direct modulation of γ-secretase activity. *J. Biol. Chem.* 278:31831–31837. http://dx.doi.org/10.1074/jbc.M303592200

Wyss-Coray, T., F. Yan, A.H. Lin, J.D. Lambris, J.J. Alexander, R.J. Quigg, and E. Masliah. 2002. Prominent neurodegeneration and increased plaque formation in complement-inhibited Alzheimer's mice. *Proc. Natl. Acad. Sci. USA.* 99:10837–10842. http://dx.doi.org/10.1073/pnas.162350199

Xu, G., H. Zhang, S. Zhang, X. Fan, and X. Liu. 2008. Plasma fibrinogen is associated with cognitive decline and risk for dementia in patients with mild cognitive impairment. *Int. J. Clin. Pract.* 62:1070–1075. http://dx.doi.org/10.1111/j.1742-1241.2007.01268.x

Yan, P., X. Hu, H. Song, K. Yin, R.J. Bateman, J.R. Cirrito, Q. Xiao, F.F. Hsu, J.W. Turk, J. Xu, et al. 2006. Matrix metalloproteinase-9 degrades amyloid-β fibrils in vitro and compact plaques in situ. *J. Biol. Chem.* 281:24566–24574. http://dx.doi.org/10.1074/jbc.M602440200

Yan, P., A.W. Bero, J.R. Cirrito, Q. Xiao, X. Hu, Y. Wang, E. Gonzales, D.M. Holtzman, and J.M. Lee. 2009. Characterizing the appearance and growth of amyloid plaques in APP/PS1 mice. *J. Neurosci.* 29:10706–10714. http://dx.doi.org/10.1523/JNEUROSCI.2637-09.2009

Yasojima, K., C. Schwab, E.G. McGeer, and P.L. McGeer. 1999. Up-regulated production and activation of the complement system in Alzheimer's disease brain. *Am. J. Pathol.* 154:927–936. http://dx.doi.org/10.1016/S0002-9440(10)65340-0

SUPPLEMENTAL MATERIAL

Czirr et al., https://doi.org/10.1084/jem.20162011

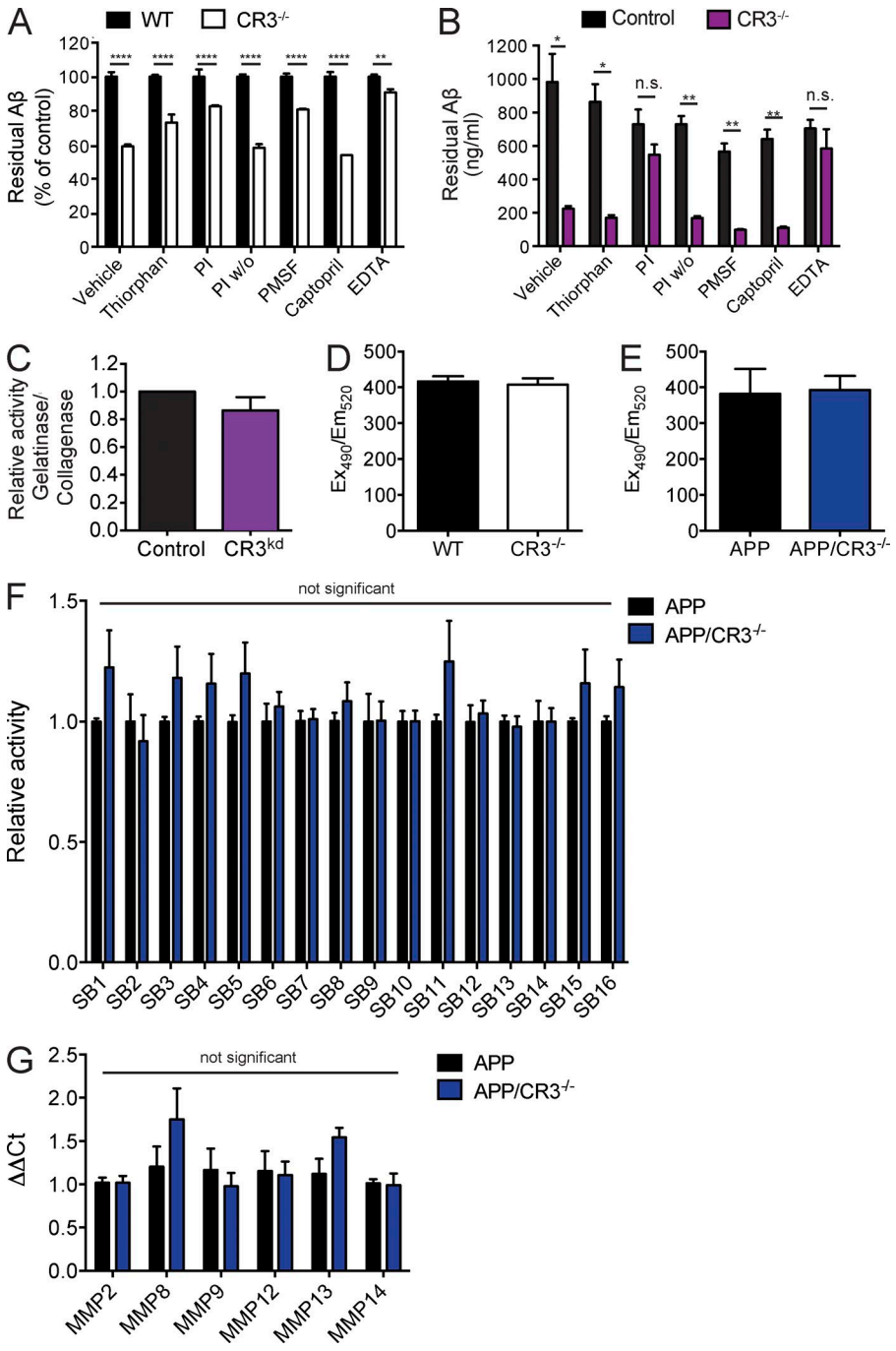

Figure S1. **MMP activity is not changed in CR3-deficient cells or mice.** (A) Cell-free Aβ degradation assay in supernatants of adult WT and CR3$^{-/-}$ microglia with addition of protease inhibitors (PI). PI w/o, protease inhibitor cocktail lacking EDTA. (B) Cell-free assay in supernatants of control and CR3^{kd} BV2 cells with addition of protease inhibitors. (A and B) Representative graphs of three independent experiments are shown. (C) Quantification of MMP2 and MMP9 activity in conditioned medium of control and CR3^{kd} BV2 cells. Combined data of two independent experiments are shown. (D) Quantification of total MMP activity in cortical lysates of WT and CR3$^{-/-}$ mice. n = 9–11 individual mice. (E) Quantification of total MMP activity in cortical lysates of APP and APP/CR3$^{-/-}$ mice. n = 6–7 individual mice. (F) Quantification of MMP profiling assay in cortical lysates of APP and APP/CR3$^{-/-}$ mice. n = 5 individual mice. (G) qPCR analysis of MMP expression in mRNA from primary adult microglia. Primary microglia are from n = 7 individual mice. All groups are male and female mice. Unpaired Student's t test was used. *, $P < 0.05$; **, $P < 0.01$; ***, $P < 0.001$. All values are mean ± SEM.

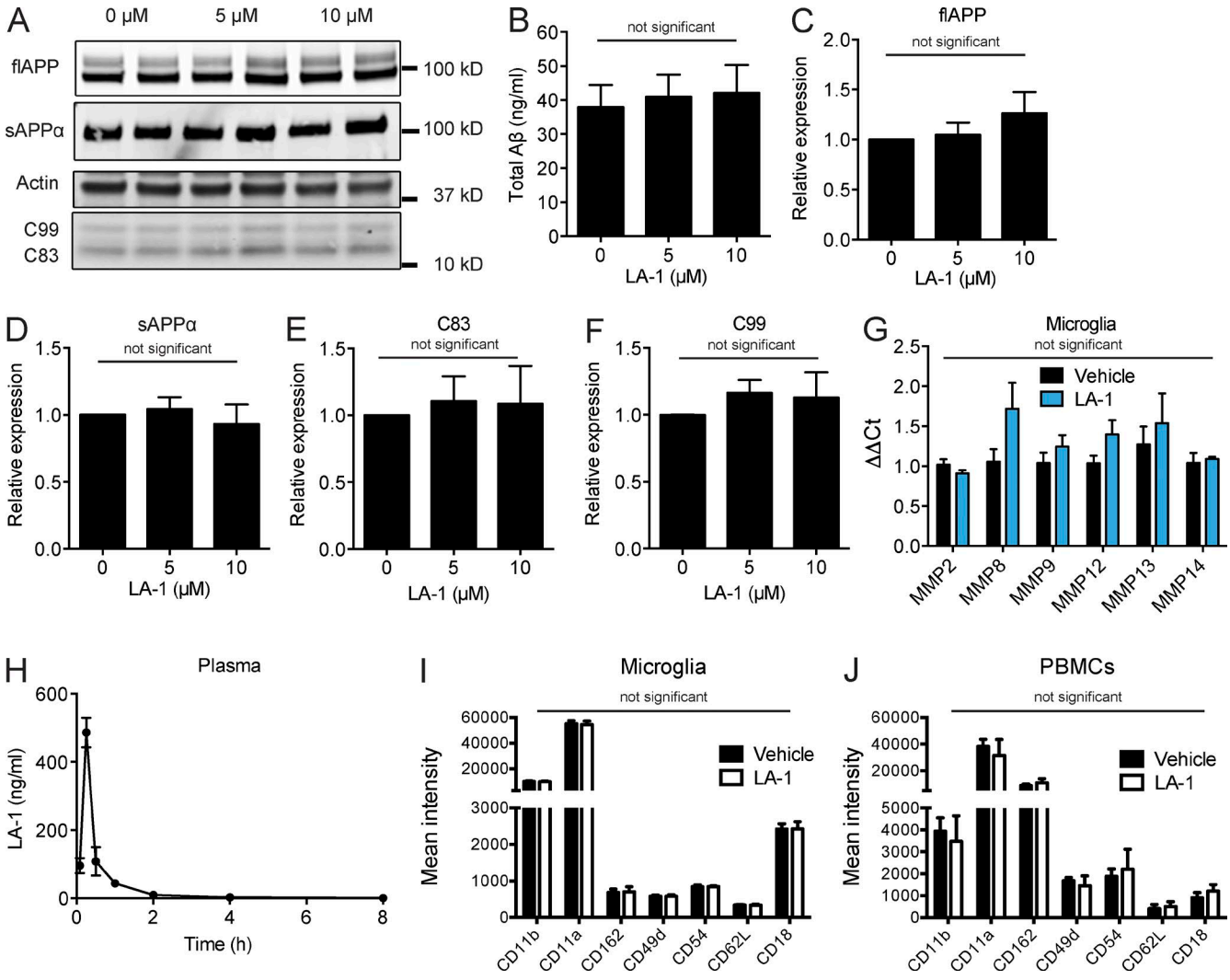

Figure S2. **LA-1 treatment does not change APP processing or expression of vascular adhesion markers on PBMCs or microglia.** (A) Representative Western blot showing APP processing in lysates and sAPPα levels in conditioned supernatants of APP-overexpressing Chinese hamster ovary cells after LA-1 treatment. flAPP, full-length APP. (B) Aβ measurements in conditioned supernatants of APP-overexpressing Chinese hamster ovary cells after LA-1 treatment. (C–F) Quantification of full-length APP and processing products after LA-1 treatment. (B–F) Data are combined from three independent experiments. (G) qPCR analysis of MMP expression in mRNA from primary adult microglia. Primary microglia are from $n = 7$ individual mice. (H) Plasma levels of LA-1 after a single injection quantified by mass spectrometry. $n = 3$ individual mice per time point, with only male mice. (I and J) Flow cytometric quantification of vascular adhesion molecule expression on primary adult microglia (I) and PBMCs (J) isolated after 10 d of LA-1 injections. $n = 5$ individual mice per group. All groups were male and female mice except for H. One-way ANOVA and Tukey's posthoc test (B–F) or unpaired Student's t test (G, I, and J) was used. All values are mean ± SEM.

Table S1. **qPCR primer sequences**

Gene	Primer sequences (5′–3′)
MMP2 for	CAAGTTCCCCGGCGATGTC
MMP2 rev	TTCTGGTCAAGGTCACCTGTC
MMP8 for	TCTTCCTCCACACACAGCTTG
MMP8 rev	CTGCAACCATCGTGGCATTC
MMP9 for	GAGACGGGTATCCCTTCGAC
MMP9 rev	TGACATGGGGCACCATTTGAG
MMP12 for	GGGCTGCTCCCATGAATGAC
MMP12 rev	CCAGAGTTGAGTTGTCCAGTTG
MMP13 for	CTTCTTCTTGTTGAGCTGGACTC
MMP13 rev	CTGTGGAGGTCACTGTAGACT
MMP14 for	GCCTTGCCTGTCACTTGTAAA
MMP14 rev	CAGTATGGCTACCTACCTCCAG
tPA for	AACGCAGACAACTTACCAACA
tPA rev	GTTCGCTGCAACTTCGGAC
IDE for	GAACGATGCCTGGAGACTCTT
IDE rev	TTCCCTTACGTCGATGCCTTC
GAPDH for	AGGTCGGTGTGAACGGATTTG
GAPDH rev	TGTAGACCATGTAGTTGAGGTCA

Abbreviations used: for, forward; IDE, insulin-degrading enzyme; rev, reverse.

Table S2. **Sequence of FRET substrates and substrate specificity for the MMP profiling kit**

Substrate	FRET peptide sequence	MMP specificity
SB1	QXL520-Pro-Leu-Gly-Leu-Trp-Ala-D-Arg-Lys(5-FAM)-NH_2	13
SB2	QXL520-Pro-Leu-Ala-Leu-Trp-Ala-Arg-Lys(5-FAM)-NH_2	1,7,8,12,13
SB3	QXL520-Pro-Leu-Gly-Cys(Me)-His-Ala-D-Arg-Lys(5-FAM)-NH_2	1,2,8,9,12,13
SB4	5-FAM-Pro-Leu-Ala-Nva-Dap(QXL520)-Ala-Arg-NH_2	1,2,7,8,12,13
SB5	5-FAM-Pro-Leu-Gly-Leu-Dap(QXL520)-Ala-Arg-NH_2	1,2,7,8,12,13
SB6	QXL520-Pro-Leu-Gly-Met-Trp-Ser-Arg-Lys(5-FAM)-NH_2	2,13
SB7	QXL520-Pro-Tyr-Ala-Tyr-Trp-Met-Arg-Lys(5-FAM)-NH_2	7,12,13
SB8	QXL520-Arg-Pro-Lys-Pro-Leu-Ala-Nva-Trp-Lys(5-FAM)-NH_2	7,12,13
SB9	QXL520-Arg-Pro-Leu-Ala-Leu-Trp-Arg-Lys(5-FAM)-NH_2	1,2,7,8,12,13
SB10	QXL520-Pro-Leu-Ala-Tyr-Trp-Ala-Arg-Lys(5-FAM)-NH_2	13
SB11	5-FAM-Pro-Cha-Gly-Nva-His-Ala-Dap-(QXL520)-NH_2	1,2,8,12,13
SB12	5-FAM-Arg-Pro-Lys-Pro-Tyr-Ala-Nva-Trp-Met-Lys(QXL520)-NH_2	1,2,3,12,13
SB13	5-FAM-Arg-Pro-Lys-Pro-Val-Glu-Nva-Trp-Arg-Lys-(QXL520)-NH_2	3,12
SB14	QXL520-γ-Abu-Pro-Cha-Abu-Smc-His-Ala-Dab(5-FAM)-Ala-Lys-NH_2	1,2,3,7,8,9,12,14
SB15	QXL520-γ-Abu-Pro-Gln-Gly-Leu-Dab-(5-FAM)-Ala-Lys-NH_2	1,2,7,8,12,13
SB16	QXL520-Arg-Pro-Lys-Pro-Gln-Gln-Phe-Trp-Lys(5-FAM)-NH_2	12,13

Abbreviation used: FRET, fluorescence resonance energy transfer.